Communication

Observation of Micro-scale Surface Morphology with Microtexture Development During Plane Strain Tensile Deformation in AZ31 Magnesium Alloy

KEUNHO LEE, KYUNG IL KIM, SE-JONG KIM, DONG-WOO SUH, KYU HWAN OH, and HEUNG NAM HAN

The change of microstructure including microtexture and surface morphology in AZ31 magnesium alloy under plane strain tension was investigated by 3D observation combined confocal microscope and high-resolution electron backscattered diffraction. Micro-scale changes in the surface morphology were observed on the area including $\{10\bar{1}2\}\langle 10\bar{1}1\rangle$ tensile twin bands. The mechanism for surface morphology variation was discussed with the nucleation of tensile twinning and the strain partitioning caused by continuing deformation after the nucleation of the twins.

DOI: 10.1007/s11661-014-2679-1

It is well known that magnesium (Mg) has a shortage of independent slip systems to accommodate plastic deformation at room temperature. This limit of operating slip systems in Mg stems from its low-symmetry hexagonal close-packed crystal structure and much higher critical resolved shear stress (CRSS) of non-basal slip modes than that of $(0001)\langle 11\bar{2}0\rangle$ basal slip.[1–7] In order to accommodate deformation on account of external forces, the deformation twinning, which has a relatively low CRSS, easily forms during plastic deformation at low temperature. Deformation twinning is a significant deformation mechanism in Mg alloys; hence much research has focused on the fundamental understanding and advanced application of several deformation twins.[8–12] Among them, $\{10\bar{1}2\}\langle 10\bar{1}1\rangle$ tensile twin is primarily observed during tensile loading along *c*-axis and accompanies the rotation of the *c*-axis by 86 deg.[8] This crystallographic rotation induces a local material flow and a complex strain state in the regions of the tensile twin, influencing a deformation texture in Mg alloys. For an accurate analysis of the strain state caused by the tensile twinning, it is necessary to investigate tensile twin regions through three dimensional (3D) observation during *in situ* deformation.

Meanwhile, many studies have utilized *in situ* electron backscattered diffraction (*in situ* EBSD) technique during deformation to elucidate deformation mechanism of various metals and alloys from their microstructural evolution at the micro-scale level.[13–15] In addition, microstructure-based computational simulations such as crystal plasticity finite element methods (CP-FEM)[16–19] and crystal plasticity fast Fourier transform-based model[13,20] have supported experimental proofs, and predicted how materials are deformed under external deformation conditions. Especially, recent investigations have used the 3D reconstructed microstructure obtained from by EBSD combined with focused ion beam, or synchrotron X-ray microtomography as an initial microstructure for the simulation.[21–23] As for the Mg alloys, a 3D CP-FEM simulation that considered both crystallographic slip and deformation twinning was done to explain the heterogeneity of the stress concentration as well as the slip and twin activities.[18,19] However, there are few experimental reports regarding 3D observation of microstructural evolution in Mg alloy based on *in situ* deformation technique.

In this study, 3D observation combined confocal microscope and high-resolution EBSD (HR-EBSD) was conducted during stepwise deformations to obtain the microtexture development and the profile of the surface height in AZ31 Mg alloy under plane strain tension. In order to understand the mechanism causing the surface height variations induced by tensile twinning, we introduced a phenomenological crystallographic model with consideration of the orientation information of the parent grain and a selection of six tensile twin variants. In addition, the surface morphology change by continuing deformation after the nucleation of tensile twinning was discussed in view of the strain partitioning effect among the parent grain and the twin bands.

An AZ31 magnesium alloy with a chemical composition of Mg-3.27Al-0.96Zn (wt pct) was cast and then homogenized at 623 K (350 °C) for 24 hour. A specially designed specimen for plane strain tension with the thickness of 300 μm was prepared using a wire cutting method.[14] The specimen was ground mechanically and then electropolished to remove the residual stress and roughness on the surface. Four rectangular micro-indents were made in the center of specimen surface for tracing the microstructure of the same area during stepwise deformations and measuring macroscopic strains at each deformation step.

Figure 1 shows a schematic diagram for the experimental process that includes stepwise plane strain tension[14] with 3D observation by HR-EBSD and confocal microscope. The device was used to elongate the specimen uniaxially as a plane strain tensile mode and set up inside a scanning electron microscope (JSM-

KEUNHO LEE and KYUNG IL KIM, Ph.D. Students, KYU HWAN OH and HEUNG NAM HAN, Professors, are with the Department of Materials Science and Engineering and RIAM, Seoul National University, Seoul 151-744, Republic of Korea. Contact e-mail: hnhan@snu.ac.kr SE-JONG KIM, Senior Researcher, is with the Material Deformation Department, Korea Institute of Materials Science Changwon, Gyeongnam 642-831, Republic of Korea. DONG-WOO SUH, Associate Professor, is with the Graduate Institute of Ferrous Technology, Pohang University of Science and Technology, Pohang 790-784, Republic of Korea.

Manuscript submitted August 6, 2014.
Article published online November 25, 2014

6500F, JEOL) chamber. The crystallographic orientation data were collected and analyzed using an EBSD software package (INCA Crystal and HKL Channel 5, Oxford Instruments). A profile of the surface morphology in the same location where the HR-EBSD scan occured was obtained by means of a confocal microscope system (VK-X100K, KEYENCE) at each deformation step. We observed several representative regions in particular including tensile twin at a high magnification mode. A comparative analysis of the surface profile between the parent grain and twin bands was conducted with a software (VK Analyzer, KEYENCE) that was provided with the confocal microscope.

Figure 2 displays the scanning electron microscope images of the AZ31 ingot at each stepwise deformation, showing the macroscopic strains calculated from the relative displacement of the four micro-indents. Based upon the values of the macroscopic strains during deformation in Figure 2(c), where the major strain was 5.3 pct and the minor strain was nearly −0.2 pct, we confirmed that the plane strain condition was maintained during tensile deformation. For the stepwise deformations corresponding to the major strains of 0, 2.5, and 5.3 pct, the crystallographic orientation maps inside the rectangular areas marked by indentation were measured using HR-EBSD.

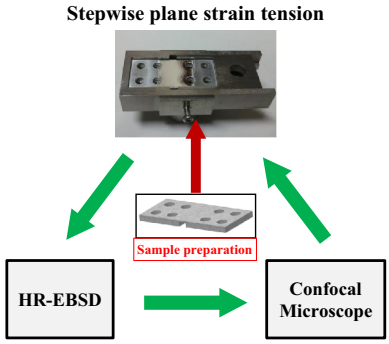

Fig. 1—Experimental process that includes stepwise plane strain tension with 3D observation combined HR-EBSD and confocal microscope.

Figure 3 shows the measured orientation image maps of the surface normal direction (ND). For grain identification, the critical misorientation angle was taken as 5 deg. Before applying deformation as shown in Figure 3(a), it was found that the microstructure consists of several coarse grains and the average grain size was 168 μm. It can be seen that deformation twinning formed at earlier stage of the plastic deformation and continued to develop as the strain increased to 5.3 pct as shown in Figures 3(b) and (c). We examined the misorientation angle between the parent and the twinned region, which revealed that all of the deformation twins had a misorientation angle in the range of 84 to 88 deg, meaning that they are $\{10\bar{1}2\}\ \langle 10\bar{1}1\rangle$ tensile twins. In order to investigate the correlation between tensile twinning and surface height variation, we selected three different regions indicated by rectangular black outlines (regions 1, 2 and 3) in Figures 3(b) and (c) and examined these regions using 3D observation combined HR-EBSD and confocal microscope at high magnification.

Figure 4 shows the magnified ND inverse pole figure maps and height displacement maps of regions 1, 2, and 3. Note that the height variation between the parent grain and the twin bands was detected in all three regions. It can be seen that the twin bands in regions 1 and 3 were higher than the areas including the parent grain, whereas the twins in region 2 were lower than the parent grain. The center top part of the height displacement map in Figure 4(b) indicated by a red circle also shows a periodic morphology change, however, any orientation change from the EBSD map could not be observed. It might be thought that tensile twin in another grain underneath the surface grain nucleates and triggers the height variation on specimen surface, considering the specimen thickness (300 μm) and the size of the grain (140 μm) in region 2. The relative height displacement profiles along the white lines shown in Figure 4 are displayed in Figure 5. An average height of each region in Figure 4 sets as reference value. From the height distributions, the tensile twins in three regions could be classified as uplifting twins (regions 1 and 3) and sinking twins (region 2). It can be confirmed that

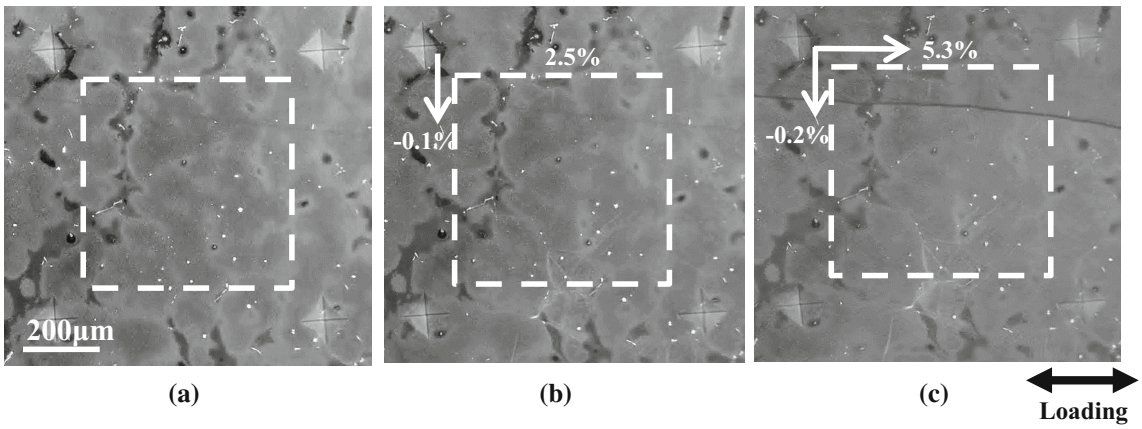

Fig. 2—SEM images of AZ31 ingot at major strains of (*a*) 0 pct, (*b*) 2.5 pct, and (*c*) 5.3 pct, calculated from relative displacements between the marked indents.

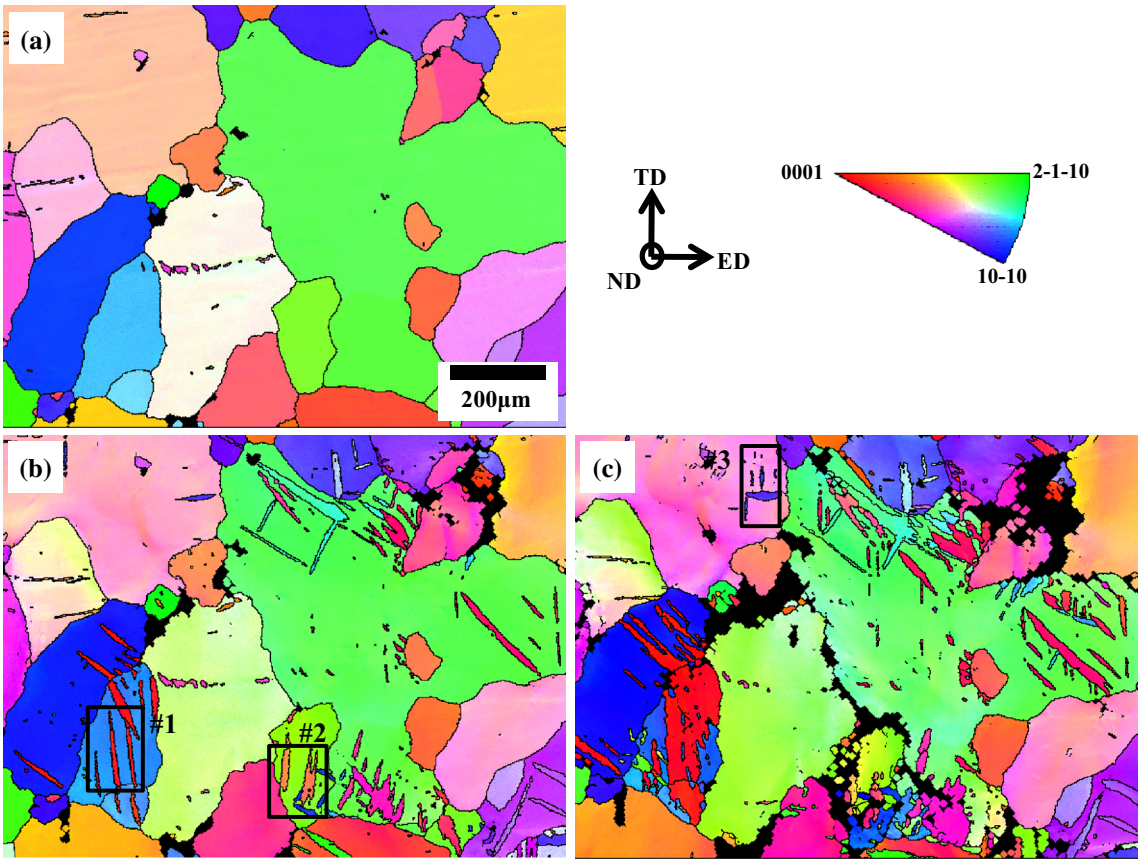

Fig. 3—Orientation map of surface normal direction at major strains of (*a*) 0 pct (*b*) 2.5 pct, and (*c*) 5.3 pct. (▬ misorientation angle > 5 deg).

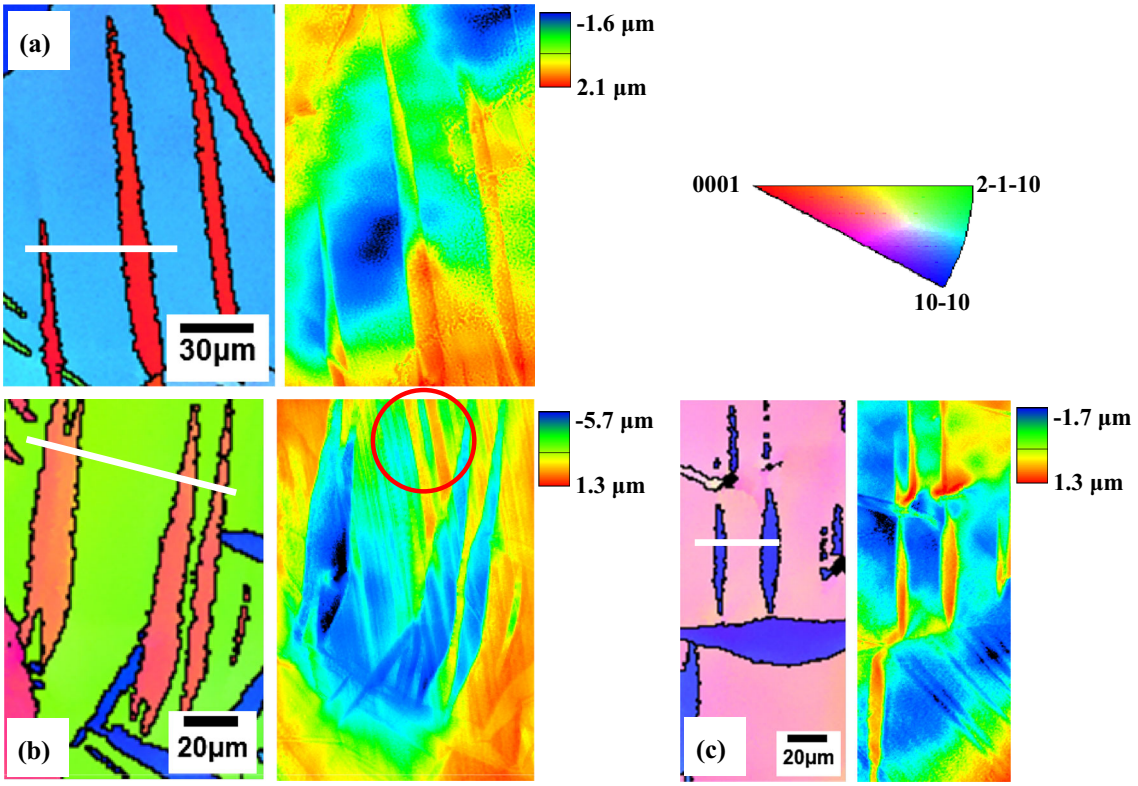

Fig. 4—Magnified orientation map of surface normal direction and height displacement map of regions (*a*) 1, (*b*) 2, and (*c*) 3 in Fig. 3.

significant micro-scale surface height variations existed on the parent grain and twin bands. This implied the generation of strain toward the ND of specimen.

In order to analyze precisely, the strain state induced by the nucleation of tensile twinning, we calculated the twinning strain tensor on the basis of specimen coordinate system. It can be calculated using the twinning strain tensor on the crystal coordinate system and the orientation matrix of the parent grain, which can be expressed as follows[24]:

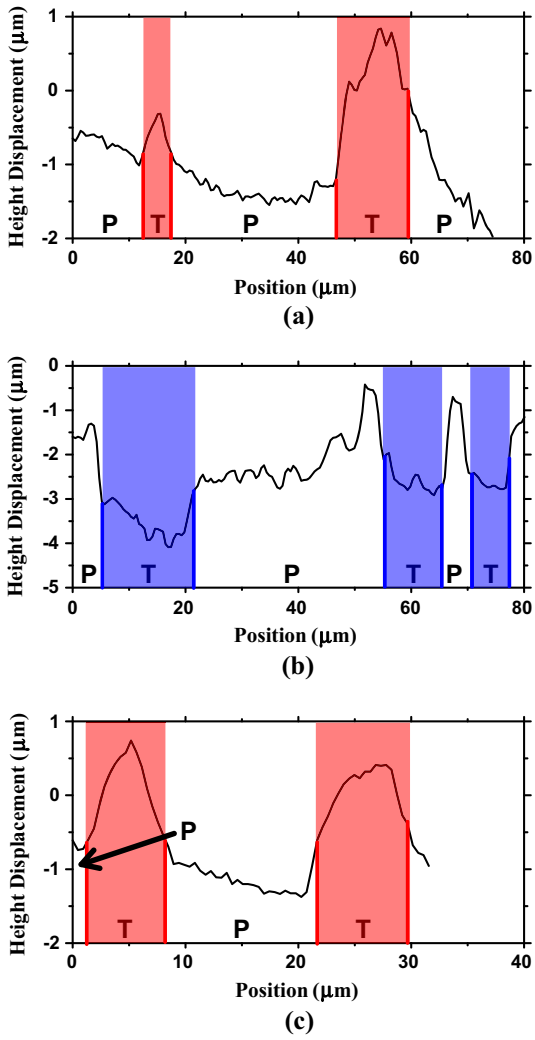

Fig. 5—Relative height displacement profiles of regions (*a*) 1, (*b*) 2, and (*c*) 3 in Fig. 3. P and T indicate the parent phase and twined phase, respectively.

$$[\varepsilon_{\text{twin}}]_{ij}^{\text{SP}} = O^{-1} \cdot [\varepsilon_{\text{twin}}]_{\text{kl}}^{\text{CR}} \cdot [O^{\text{T}}]^{-1}, \quad [1]$$

where $[\varepsilon_{\text{twin}}]_{kl}^{\text{SP}}$ is the twinning strain tensor on the specimen coordinate system, O is the orientation matrix of the parent grain, and $[\varepsilon_{\text{twin}}]_{ij}^{\text{CR}}$ is the twinning strain tensor on the crystal coordinate system. $[\varepsilon_{\text{twin}}]_{ij}^{\text{CR}}$ can be determined as one of the six variants of the tensile twinning. The twin variant which had the least misorientation angle with the real twin phase measured by HR-EBSD was chosen from the six variants of tensile twinning. The twinning strain tensor on the specimen coordinate system was calculated using Eq. [1] with the selected variant of tensile twinning.

The calculated normal strain toward the surface direction by tensile twinning ($\varepsilon_{33}^{\text{SP}}$) for three regions is listed in Table I with the tensile twin types based on surface height measurements. In regions 2 and 3, both the calculated normal strain and the measured tensile twin type show the same aspects qualitatively, whereas the calculated normal strain (sinking twin) differs from measured surface height profile (uplifting twin) in region 1. It could imply that, in the case of region 1, other factors affected the height variation between the parent grain and the twin bands in addition to the nucleation of the tensile twinning. It is noted that, since our experimental procedures were kept up with stepwise tensile deformation, the continuing plastic deformation on the parent grain and the twin bands must have been applied after the tensile twinning.

The tensile twin and basal slip were the main deformation modes during stepwise plane strain tension. This indicates that the basal slip might be heterogeneously activated in the parent grain and the twin bands by continuing tensile deformation after the tensile twinning. To analyze the strain partitioning in the parent grain and the transformed twin bands after twining, the difference in the Schmid factor for the basal slip between them should be calculated. Table I gives the Schmid factors for the basal slip of parent grains and twin bands in three regions under plane strain tension. The Schmid factors for basal slip of the parent grain and twin bands in regions 2 and 3 were almost identical. Whereas, in region 1, the Schmid factor in the parent grain (0.32) was distinctly higher than that in the twin bands (0.22). For the elaborate analysis of the deformation modes of the parent grain in region 1, we calculated the yield stress for basal slip and tensile twinning based on Schmid's Law $\sigma_0 = \tau_{\text{CRSS}}/m$.[25] Here, τ_{CRSS} is the CRSS and m is the Schmid factor. The CRSSs for basal slip and tensile twinning in AZ31

Table I. Calculated Normal Strain Toward Surface Normal Direction by Tensile Twinning, Tensile Twin Type Based on Surface Height Measurements, and Schmid Factor of Basal Slip of Parent Grain and Twin Bands in Three Regions Under Plane Strain Tension

Region	Calculated Normal Strain, e_{33}^{SP} (pct)	Tensile Twin Type	Schmid Factor Of Parent Grain	Schmid Factor of Twin Bands
#1	−1.12	uplifting twin	0.32	0.22
#2	−1.34	sinking twin	0.43	0.44
#3	2.84	uplifting twin	0.46	0.44

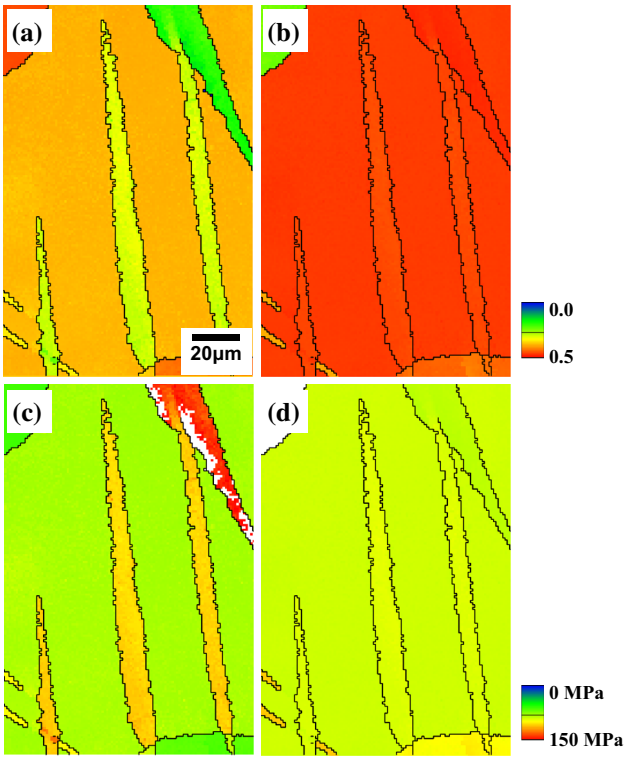

Fig. 6—Schmid factor and yield stress maps of regions 1: (*a*) and (*c*) basal slip; (*b*) and (*d*) tensile twinning.

were used as 20 and 30 MPa, respectively.[7] Figure 6 shows the Schmid factor and the yield stress maps for basal slip and tensile twinning on region 1. The mean values of σ_0 for basal slip and tensile twinning of the parent grain are obtained as 63.2 and 67.7 MPa, respectively. From the similar values of σ_0, the basal slip on the parent grain in region 1 must be activated at the further deformation with the thickening of tensile twins. Besides the yield stresses for basal slip and tensile twinning, size difference on the parent grain and the twin bands might also affect the strain partitioning after twinning. In terms of size effects, the continuing plastic deformation after onset of the twinning in region 1 concentrates on the parent grain because the size for the twin bands is much smaller than that of the parent matrix. Therefore, from the viewpoint of the strain partitioning effect, the twin bands could be relatively high comparing to the parent grain in region 1, which coincides well with the relative profile of height displacement in Figure 5(a).

Though the tensile twin in region 1 was a sinking twin from the calculation of ε_{33}^{SP}, the absolute value of the calculated normal strain (1.12 pct) was so small that the tensile twinning could not have had a profound effect upon the surface morphology. Therefore, the strain concentration on the parent grain in region 1 could induce the thickness reduction, resulting in an uplifting twin. Consequently, both the tensile twinning and strain partitioning should be synthetically considered to understand the height distribution during deformation. It is appropriate to mention that the latest 3D simulation techniques should be needed as a follow-up study, in order to investigate the twinning strain and strain partitioning effect for further analysis.

To summarize, the change of microtexture and surface morphology in the AZ31 Mg alloy during stepwise plane strain tension was investigated by 3D observation combined HR-EBSD and confocal microscope. From the microstructural evolution, $\{10\bar{1}2\}\langle 10\bar{1}1\rangle$ tensile twinning accommodated the applied plane strain deformation. Micro-scale changes in the surface morphology were observed on the region including the tensile twin bands. The calculation of the twinning strain can qualitatively capture the nature of surface height variation depending on the selected variant of tensile twinning. However, the contribution from the strain partitioning between parent grain and the twin band becomes important when there is considerable difference in the accommodation of deformation after the formation of the twin.

This work was supported by the Basic Science Research Program through the National Research Foundation of Korea (NRF) funded by the Ministry of Science, ICT and Future Planning (NRF-2013R1A2A2A01008806).

REFERENCES

1. B.L. Mordike and T. Ebert: *Mater. Sci. Eng., A*, 2001, vol. 302, pp. 37–45.
2. M.T. Perez-Prado and O.A. Ruano: *Scripta Mater.*, 2002, vol. 46, pp. 149–55.
3. M. Easton, A. Beer, M. Barnett, C. Davies, G. Dunlop, Y. Durandet, S. Blacket, T. Hilditch, and P. Beggs: *JOM*, 2008, vol. 60, pp. 57–62.
4. S.R. Agnew and J.F. Nie: *Scripta Mater.*, 2010, vol. 63, pp. 671–73.
5. Q.D. Wang, W.H. Chen, W.J. Ding, Y.P. Zhu, and M. Mabuchi: *Metall. Mater. Trans. A*, 2001, vol. 32A, pp. 787–94.
6. S. Jeong, J. Park, I. Choi, and S.H. Park: *Korean J. Met. Mater.*, 2013, vol. 51, pp. 701–11.
7. S.R. Agnew, D.W. Brown, and C.N. Tome: *Acta Mater.*, 2006, vol. 54, pp. 4841–52.
8. J. Koike, Y. Sato, and D. Ando: *Mater. Trans.*, 2008, vol. 49, pp. 2792–800.
9. J.H. Shin, S.H. Kim, T.K. Ha, K.H. Oh, I.S. Choi, and H.N. Han: *Scripta Mater.*, 2013, vol. 68, pp. 483–86.
10. J.H. Park, H.L. Kim, J.E. Jung, and Y.W. Chang: *Met. Mater. Int.*, 2013, vol. 19, pp. 389–98.
11. J. Scott, M. Miles, D. Fullwood, B. Adams, A. Khosravani, and R.K. Mishra: *Metall. Mater. Trans. A*, 2013, vol. 44A, pp. 512–16.
12. B. Clausen, C.N. Tome, D.W. Brown, and S.R. Agnew: *Acta Mater.*, 2008, vol. 56, pp. 2456–68.
13. D.H. Kim, S.J. Kim, S.H. Kim, A.D. Rollett, K.H. Oh, and H.N. Han: *Acta Mater.*, 2011, vol. 59, pp. 5462–71.
14. Y.S. Choi, K.I. Kim, K.H. Oh, H.N. Han, S.H. Kang, J. Jang, and J.H. Han: *J. Mater. Res.*, 2013, vol. 28, pp. 2829–34.
15. K. Lee, S.J. Park, Y.S. Choi, S.J. Kim, T.H. Lee, K.H. Oh, and H.N. Han: *Scripta Mater.*, 2013, vol. 69, pp. 618–21.
16. R. Becker, J.F. Butler, H. Hu, and L.A. Lalli: *Metall. Trans. A*, 1991, vol. 22, pp. 45–58.

17. Z. Zhao, S. Kuchnicki, R. Radovitzky, and A. Cultino: *Acta Mater*., 2007, vol. 55, pp. 2361–73.
18. S.H. Choi, D.W. Kim, B.S. Seong, and A.D. Rollett: *Int. J. Plast*, 2011, vol. 27, pp. 1702–20.
19. J. Zhang and S.P. Joshi: *J. Mech. Phys. Solids*, 2012, vol. 60, pp. 945–72.
20. R.A. Lebensohn: *Acta Mater*., 2001, vol. 49, pp. 2723–37.
21. S. Schmidt, S.F. Nielsen, C. Gundlach, L. Margulies, X. Huang, and D.J. Jensen: *Science*, 2004, vol. 305, pp. 229–32.
22. M.D. Uchic, M.A. Groeber, D.M. Dimiduk, and J.P. Simmons: *Scripta Mater*., 2006, vol. 55, pp. 23–28.
23. R.A. Lebensohn, R. Brenner, O. Castelnau, and A.D. Rollett: *Acta Mater*., 2008, vol. 56, pp. 3914–26.
24. S.H. Hong, H.T. Jeong, C.H. Choi, and D.N. Lee: *Mater. Sci. Eng., A*, 1997, vol. 229, pp. 174–81.
25. E. Schmid and W. Boas: *Plasticity of Crystals with Special Reference to Metals*, F.A. Hughes, London, United Kingdom, 1950.